THE EFFECTS OF A MAGNETIC FIELD ON ABUNDANCE DETERMINATIONS IN STELLAR ATMOSPHERES

by 4589

CHARLES STEPHEN NICHOLS

B. S., University of Missouri at Rolla, 1968

A MASTER'S THESIS

submitted in partial fulfillment of the

requirements for the degree

MASTER OF SCIENCE

Department of Physics

KANSAS STATE UNIVERSITY
Manhattan, Kansas

1970

Approved by:

J. C. Evans
Major Professor

TABLE OF CONTENTS

THIS BOOK CONTAINS NUMEROUS PAGES WITH DIAGRAMS THAT ARE CROOKED COMPARED TO THE REST OF THE INFORMATION ON THE PAGE.

THIS IS AS RECEIVED FROM CUSTOMER.

ILLEGIBLE DOCUMENT

THE FOLLOWING DOCUMENT(S) IS OF POOR LEGIBILITY IN THE ORIGINAL

THIS IS THE BEST COPY AVAILABLE

I. INTRODUCTION

From the coarse and fine atmospheric analysis of several of the peculiar A stars (Renson 1967), it has been found that apparent abundance anomalies exist for certain elements. This group of stars covers the spectral type from B8 to F0 and they more or less lie on the main sequence. In 1946, Babcock began a search from Mt. Wilson and later Palomar for stars with observable magnetic fields, which resulted in the publication of a catalogue of magnetic star observations (Babcock 1958). In this catalogue, Babcock lists 89 stars as definitely showing the inverse longitudinal Zeeman effect and hence possessing a magnetic field in the line formation region. Preston (1967) has begun an observational program for magnetic stars at Lick Observatory patterned after Babcock's work, and has in general obtained similar but not identical results for stars common to both programs. Some or all of the differences could be due to observational procedures or intrinsic stellar variations. Stellar magnetic fields of from 100 to 34000 gauss have been measured by Preston and Babcock. The average value of these fields is about 2000 gauss, and all fields detected seem to be variable. Approximately 70 of the 89 stars listed by Babcock as having magnetic fields turn out to be Ap stars. The abundance anomalies mentioned previously can roughly be divided into three groups defined by the element being: (i) underabundant (C,O); (ii) of normal abundance or slightly overabundant (iron peak group, Si); (iii) very overabundant (rare earths). The suggestion has been made by Babcock (1949) that magnetic intensification in stellar absorption lines might give rise to the observed overabundances in the Ap stars.

In the investigation to be described, the magnitude of the overabundance due to line intensification by Zeeman broadening was estimated from theoretical curves of growth for lines of C I, Si I, Si II, Fe I, Fe II, and Eu II for a grid of ten model atmospheres. These atmospheres range in spectral type from approximately A0 to F0.

II. THE MODEL ATMOSPHERES

In this investigation the usual assumptions of a homogeneous, steady-state, plane-parallel atmosphere in hydrostatic equilibrium have been made. The assumption has also been made that the conditions for local thermodynamic equilibrium are satisfied. The scheme used in the computation of the model atmosphere was developed by Weidemann (1955) and later modified by Elste (1968). The digital computer program which was used in the computations was written by Elste and modified by Evans (1970). The logarithm of the continuum optical depth at 5000 Å is used as the independent depth variable. Neglecting helium ionization and molecular formation, the ionization equilibrium is computed by applying the Saha equation to each of the most abundant elements. Several elements of similar ionization potential are considered together in the ionization equilibrium by using the ionization potential and partition functions of the most abundant and adding their abundances. This process reduces the computations while maintaining the accuracy in determining the electron pressure. Table 1 gives the adopted atmospheric abundances used in this study which are the solar abundances. The secondary elements are shown in parentheses, and ε is the ratio of the number density for the element group in question relative to that for H.

The primary sources of continuous absorption are bound-free and free-free absorption by hydrogen in the form H, H^-, and H_2^+. The secondary sources are the bound-free and free-free absorption by several neutral metals, which are treated using a hydrogenic approximation and integrating over all absorption edges rather than summing over them. Instead of calculating a temperature distribution by enforcing flux constancy at each layer in the atmosphere, we have chosen to adopt one from the literature. Thus for a given chemical composition, effective surface gravity, and the chosen temperature distribution, our atmosphere computation consists of the computation of a pressure-opacity-surface flux model. A more detailed description of the model atmosphere is given in Appendix A.

TABLE 1

ADOPTED ATMOSPHERIC ABUNDANCES FOR THE MODEL COMPUTATIONS

Element	log ε	Element	log ε
H(O,N)	0.0004	K	-7.3000
He	-0.8240	Ca	-6.1200
C(S,P)	-3.1160	Cr(Ti,V)	-6.0900
Na	-5.7000	Fe(Co,Cu)	-5.5700
Mg	-4.6000	Ni(Mn)	-6.0900
Si	-4.5000		

The temperature distributions for the atmospheres used in this study were taken from a grid of model atmospheres calculated by Mihalas (1965a), where the condition of radiative equilibrium was enforced using a modification of the temperature correction scheme devised by Avrett and Krook (1963). The possibility of using a grid of convective model atmospheres (Mihalas 1965b) or a scaled solar approach (Gingerich 1969) was also considered. Each of these approaches gives essentially the same surface flux over the visible spectrum. Glagolevskii (1967) argues that convection is important in the atmospheres of the Ap stars, but in a recent article Durrant (1970) contends that the atmospheric structure of the Ap stars is identical to that for normal A stars. Since there was no real evidence in favor of the convective models they were not used. The use of a scaled solar model was rejected, because the main opacity source for models one through four is different from that of the sun. The temperature distributions calculated by Mihalas were used in a model atmosphere program and the pressure-opacity-surface flux models were compared with the ones obtained by Mihalas. The agreement obtained was satisfactory. As a further check on the model atmospheres H_β and H_γ were calculated for each model by using the David formulation of the hydrogen line absorption coefficient (David 1961). The hydrogen line profiles calculated were in agreement within 2% with those calculated by Mihalas.

The grid of model atmospheres used in this study is listed in Table 2 where the ratio of the number abundance of He to H was taken to be 0.15, and the logarithm of the number abundance of hydrogen to that of the metals was taken to be 3.2306. The effective surface gravities chosen are typical of those found in the Ap stars (Basheck and Oke 1965, Wolff 1968). Table 2 lists in successive columns; the model number, θ_{eff}, logarithm of the effective surface gravity, the Balmer discontinuity, the spectrophotometric gradient at λ = 5000 Å, and the approximate spectral type. The temperature-pressure-opacity models are given in Tables A1, A2, A3, A4, and A5.

TABLE 2

THE GRID OF MODEL ATMOSPHERES

Model Number	θ_{eff}	log g	D	$\phi(\mu m)$ λ 5000	Approximate Spectral Type
1	0.50	3.50	0.57	0.98	A0
2	.50	4.00	.55	1.01	A0
3	.55	3.50	.60	1.05	A2
4	.55	4.00	.56	1.08	A2
5	.60	3.50	.55	1.18	A4
6	.60	4.00	.50	1.22	A4
7	.65	3.50	.46	1.35	A7
8	.65	4.00	.40	1.38	A7
9	.70	3.50	.34	1.52	F0
10	0.70	4.00	0.29	1.54	F0

III. THE CALCULATION OF THEORETICAL CURVES OF GROWTH

The form of the curve of growth we have chosen to use is a plot of the saturated equivalent width W as ordinate against the unsaturated equivalent width W^* as defined by Aller, Elste, and Jugaku (1957) as abscissa. The saturated equivalent width is obtained by integrating over theoretical line profiles, while the unsaturated equivalent width is given by the expression

$$\log (W/\lambda)^* = \log \varepsilon + \log C_\lambda \quad (1)$$

where

$$\log C_\lambda = \log \; gf\lambda \; + \; \log L_\lambda \; (\chi) \quad (2)$$

and L_λ is an obvious modification of the definition by Aller, Elste, and Jugaku. The quantity ε as before is the relative number density of the atomic species of interest to that of hydrogen.

The theoretical profiles in flux were calculated for an LTE line formation mechanism using a modification by Evans (1969) of the gradient method proposed by Gussman (1967). The computer programs used in these calculations were developed by Evans (1969). The assumption has been made that the gradients of the line and continuum source functions are equal. The variable of integration is the logarithm of the optical depth at 5000 Å, x. The broadening mechanisms included in the line calculation are random thermal motions, natural broadening, quadratic Stark effect due to electrons and ions, van der Waals interactiions with hydrogen and helium, and the Zeeman effect. Microturbulence broadening can also be included in the calculations but it has been neglected in this investigation since it is the Zeeman broadening which is of primary interest.

The available formulas for the relative intensities of the various emission Zeeman components are only applicable in the case of absorption lines for which there is complete separation of the components and saturation is not important. Theories for the formation of absorption lines in a homogeneous magnetic field with arbitrary orientation to the line-of-sight have been developed by Unno (1956) and Stepanov (1958a, 1958b). Unno uses Stokes parameters to describe the stellar radiation field, while Stepanov considers its description in terms of two independent beams of opposite rotary polarization. Stepanov (1960) and Rachkovsky (1961) have shown the equivalence of the two theories for LTE. Extensions of Unno's work have been made by Moe (1968) and Beckers (1969).

For our calculations, we have employed a modification of Stepanov's work by Evans (1969). Besides the LTE line formation mechanism, it allows for the broadening of each Zeeman component by the other broadening mechanisms discussed above, so that, even for a reasonably large field strength the components remain unresolved. Denoting the two polarized beams by + and − , the line depth, R, for the total radiation can be expressed as

$$R = \int_{-\infty}^{+\infty} R_\lambda(x)\, Q(\tau_\lambda, \tau_\pm, \Delta\lambda)\, dx \tag{3}$$

where

$$R_\lambda = \frac{2}{F_\lambda(0)} \left[\frac{dB_\lambda}{dx}\right] E_3(\tau_\lambda) \tag{4}$$

$$Q = 1 - \left[\frac{\frac{1}{2}\left[E_3(\tau_+) + E_3(\tau_-)\right]}{E_3(\tau_\lambda)} \right] \tag{5}$$

where τ_λ is the continuum optical depth, $\tau_\pm$ is the line optical depth for each beam, and E_3 is the third exponential integral function, and F_λ is the emergent continuum flux.

The line absorption coefficient per hydrogen particle is related to Stepanov's atomic absorption coefficient for a transition with i violet (σ_V) or red (σ_R) sigma-components and j pi-components (π) by the number density of absorbing particles N, the number density of hydrogen particles N_H, and the correction for stimulated emission

$$\kappa_{\pm} = \left[1-10^{-\chi_\lambda \theta}\right] \frac{N}{N_H} \frac{\sqrt{\pi} e^2}{mc^2} \frac{f\lambda^2}{\Delta\lambda_D} \Psi_{\pm} \tag{6}$$

where
$$\Psi_{\pm} = \frac{1}{2}\left[H_{\sigma_V}+H_{\sigma_R}\right] + \frac{1}{4}\left[2H_{\pi}-H_{\sigma_V}-H_{\sigma_R}\right] \sin^2\gamma$$
$$\pm \frac{1}{2}\left[\frac{1}{4}\left[2H_{\pi}-H_{\sigma_V}-H_{\sigma_R}\right]^2 \sin^4\gamma + \left[H_{\sigma_V}-H_{\sigma_R}\right]^2 \cos^2\gamma\right]^{1/2} , \tag{7}$$

$$H_{\sigma_V} = \sum_i x\, H(a, v+v_{mag}) , \tag{8a}$$

$$H_{\pi} = \sum_j y\, H(a, v+v_{mag}) , \tag{8b}$$

$$H_{\sigma_R} = \sum_i z\, H(a, v+v_{mag}) , \tag{8c}$$

where H is the Voigt function for each Zeeman component, x, y, z, are the relative intensities, γ is the angle field lines make with the line-of-sight, and v_{mag} is the shift in Doppler width due to the magnetic field and $v = \Delta\lambda/\Delta\lambda_D$. The line optical depth is thus obtained by integrating the ratio of the line absorption coefficient to the continuum absorption coefficient in the usual fashion (Aller 1963).

The half-width of the dispersion profile contribution to the Voigt function is given by

$$a = \frac{\Gamma \lambda^2}{4\pi c\, \Delta\lambda_D} \tag{9}$$

where $$\Gamma = \Gamma_R + \Gamma_S + \Gamma_W \tag{10}$$

where the total damping half-width Γ is the sum of radiation damping, quadratic Stark effect, and van der Waals broadening. The radiation damping constants were computed with the classical relation. The depth-dependent quadratic Stark and van der Waals broadening were obtained as explicit functions of temperature and pressure from the Lindholm relations (Aller 1963). The quadratic Stark interaction constant C4 was evaluated for individual lines from experimental measurements or theoretical calculations by Griem (1964).

IV. MAGNETIC INTENSIFICATION EFFECTS

The procedure employed to study magnetic intensification was to calculate a curve of growth for a particular line and a particular atmospheric model with no magnetic field by varying the abundance of the element. This produces a curve of growth similar to those used in the observational determination of element abundances. Next we compute a curve of growth for the same line and same model allowing for Zeeman broadening by a homogeneous magnetic field of various strengths and angles relative to the line-of-sight. For a given abundance these two curves of growth have the same abscissa, but in the saturated portion the magnetic field has raised the curve by delaying the onset of optical saturation. There is no intensification in the linear portion of the curve since the line is not saturated and in the damping part pressure broadening dominates the Zeeman splitting so that the two curves are again identical. This shift in ordinate is used to determine the maximum overabundance that could result for weak and medium strong lines lying on the flat part of the curve due to magnetic intensification. Since most analyses involve line data which is entirely or predominantly in this part of the curve of growth, magnetic intensification can produce spurious results. The exact behavior of the curve depends also on the angle with the line-of-sight, since there is no intensification for the longitudinal effect for a normal triplet, and the intrinsic splitting pattern for the transition of interest.

Many of the qualitative and some of the quantitative aspects of magnetic intensification have been discussed in the literature (see Bray and Loughhead 1964, Preston 1967, Renson 1967, and Moe and Maltby 1968), but there is still a certain degree of uncertainty as to the exact quantitative behavior.

An example of magnetic intensification in the curve of growth is shown in Figure 1 in which the solid line represents the curve of growth for thermal and pressure broadening only and the dashed curve has in addition a transverse field of 2000 G. The computations are for the Fe I (152) λ4210.35 line. The splitting pattern of this and other lines used in this study is given in Table 3. The table lists in successive columns the element, multiplet number, wavelength, excitation potential, logarithm of the gf-value, and the splitting pattern. The references for the f-values are given below the table. These lines were chosen because most of them are observed in the Ap stars.

The λ4210.35 line shows no appreciable intensification as the field is increased from 2000 to 4000 G. Other lines used in this study continue to show an intensification for magnetic field strengths of up to 8000 G, which is the largest value of magnetic field we considered. Figure 2 gives the curve of growth for Fe II (27) λ4273.32. This figure shows the intensification for various field strengths in the transverse effect for model number 2.

The dependence of the magnetic intensification on z-value (Babcock 1962), excitation potential, angle between magnetic field direction and line-of-sight, and number of components in the anomalous inverse Zeeman effect has been examined. The dependence on z-value is shown graphically in Figure 3. The intensification increases while the Zeeman components are being split, but when these components become separated increasing the magnetic field does not appreciably increase the equivalent width. Figure 3 shows that a larger z-value will give a greater intensification effect for all values of magnetic field strength. The difference in z-value is not as important when the magnetic field has separated the Zeeman components.

EXPLANATION OF PLATE I

Fig. 1. - Theoretical curves of growth are shown for the Fe I (152) λ4210.35 line for thermal and pressure broadening only (solid line) and the addition of a 2000 G transverse field (dashed line). The behavior of points on the curves for a 2000 G longitudinal field (x) and a 4000 G transverse field (▲) are also shown.

PLATE I

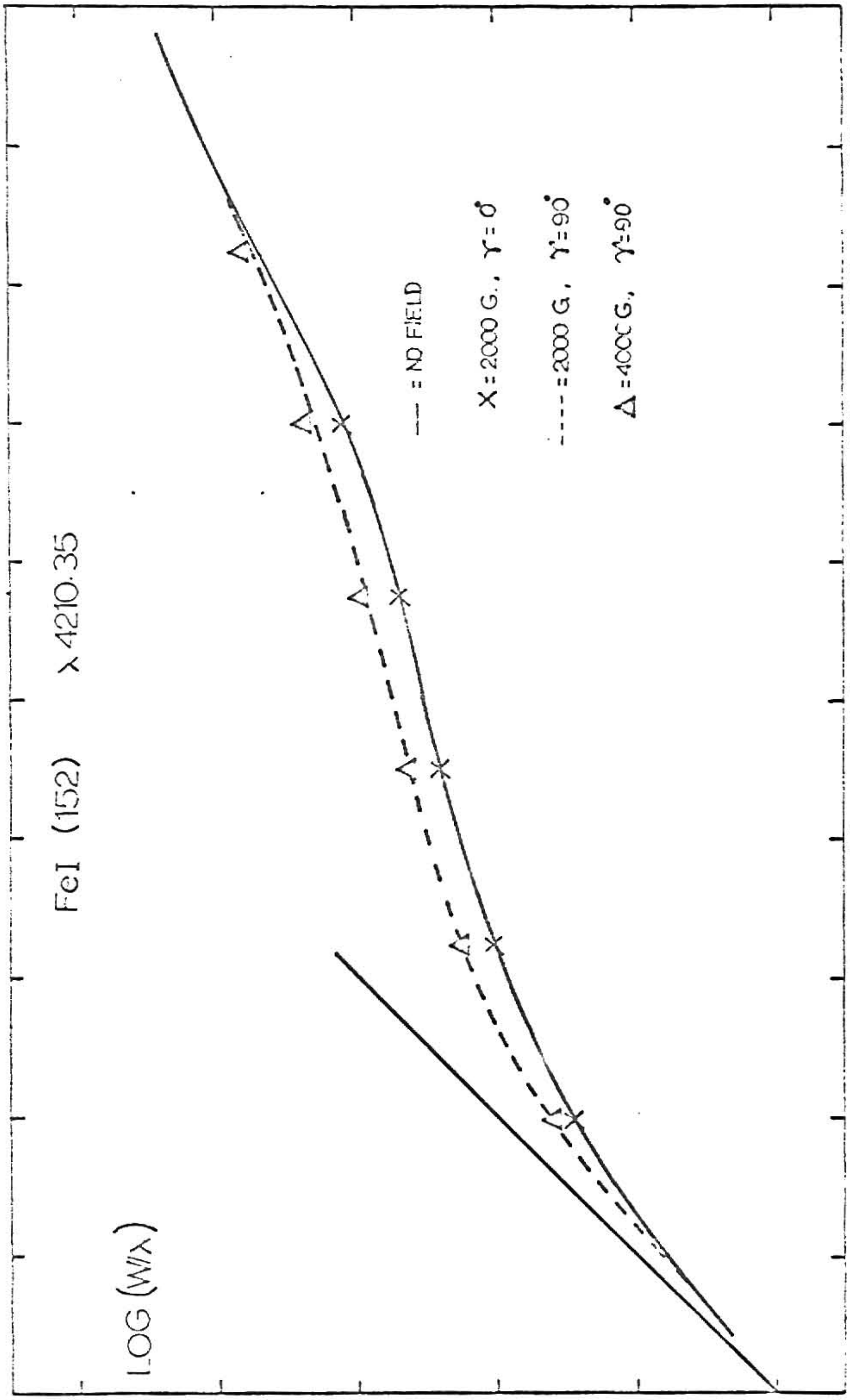
MODEL No. 8
FeI (152)
λ 4210.35
— = NO FIELD
X = 2000 G., γ = 0°
---- = 2000 G., γ = 90°
Δ = 4000 G., γ = 90°
LOG (W/λ)
LOG (W/λ)*
-3.8
-4.2
-4.6
-5.0
-5.4
-5.8
-5.4
-5.0
-4.6
-4.2
-3.8
-3.4
-3.0
-2.6
-2.2

TABLE 3

LINES USED IN THE COMPUTATIONS

Element	Mult.	λ(A)	E.P.(eV)	log gf	Splitting Pattern
C I	6	4771.72	7.46	-1.70[d]	(0.00) 1.50
Si I	3	3905.53	1.90	-1.00[c]	(0.00) 1.00
Si I	10	5690.47	4.91	-1.86[c]	(0.00) 1.50
Si II	1	3862.59	6.83	-0.90[c]	(0.07) 0.73 0.87
Fe I	2	4471.68	0.11	-5.14[b]	(0.00) 1.50
Fe I	152	4210.35	2.48	-0.19[b]	(0.00) 3.00
Fe II	27	4273.32	2.69	-2.27[e]	(0.87) 0.87 2.60
Eu II	5	3907.10	0.21	0.03[a]	(0.00 0.34 0.67) 1.33 1.67 2.00 2.33 2.67

a - Corliss and Bozman (1962)

b - Corliss and Tech (1968)

c - Wiese, Smith, and Miles (1969)

d - Wiese, Smith, and Glennon (1966)

e - Warner (1967)

EXPLANATION OF PLATE II

Fig. 2. - Theoretical curves of growth are shown for the Fe II (27) λ4273.32 line for thermal and pressure broadening only (solid line) and the addition of a microturbulent velocity of 2 km/s (x). The effect of magnetic broadening is also shown for transverse fields of 2000 G (dashed curve), 4000 G (●), and 6000 G (▲).

PLATE II

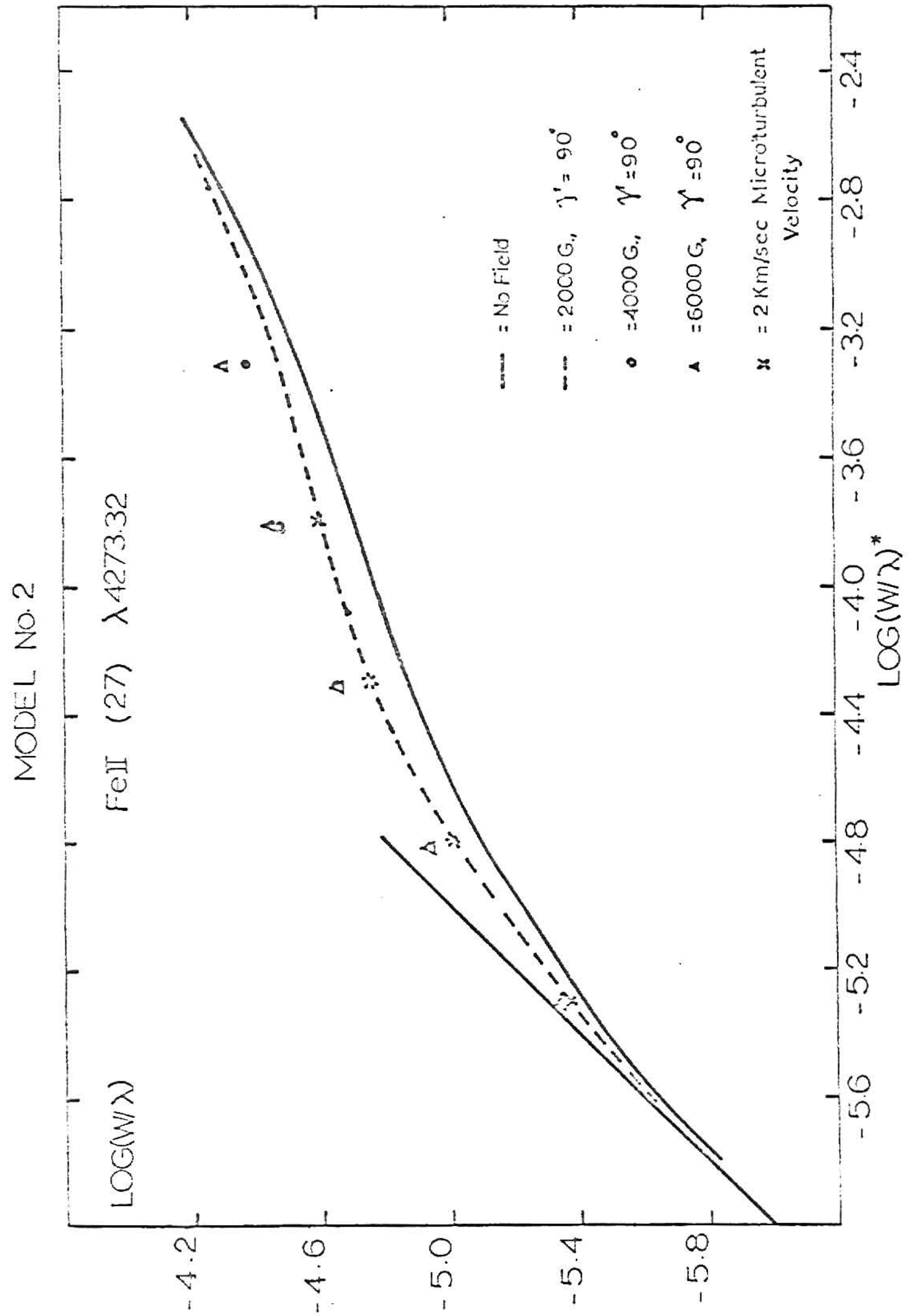
MODEL No. 2
FeII (27) λ4273.32
LOG(W/λ)
-4.2
-4.6
-5.0
-5.4
-5.8
-5.6
-5.2
-4.8
-4.4
-4.0
-3.6
-3.2
-2.8
-2.4
LOG(W/λ)*
= No Field
= 2000 G., γ' = 90°
= 4000 G., γ' = 90°
= 6000 G., γ' = 90°
= 2 Km/sec Microturbulent Velocity

EXPLANATION OF PLATE III

Fig. 3. - Magnetic intensification (W'/W) is shown as a function of magnetic field strength for the Fe I λ4210.35 line. The actual z-value (solid line) and one-half the actual z-value (dashed line) is used as a parameter.

PLATE III

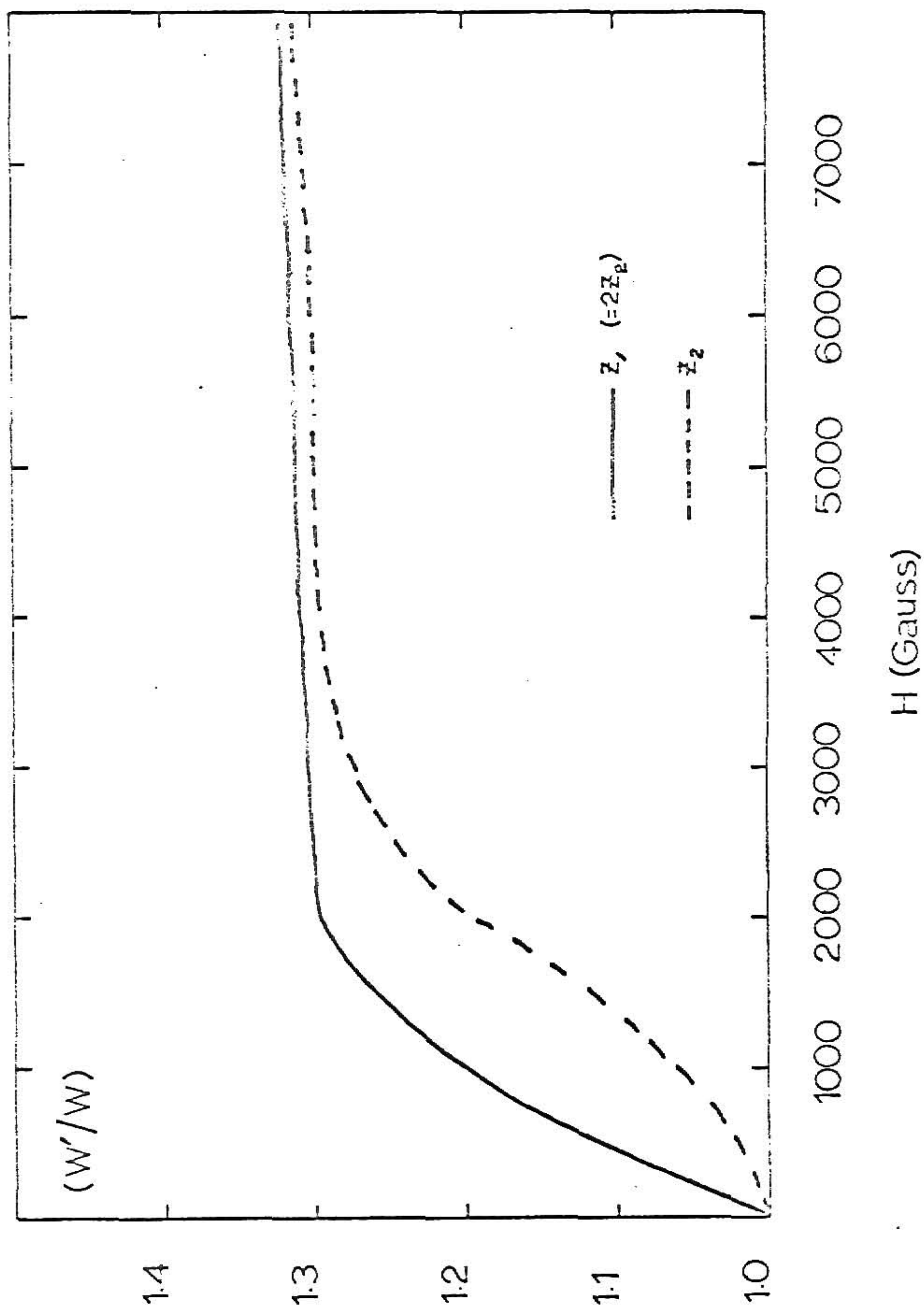

The dependence of magnetic intensification on excitation potential was studied using seven Fe I triplet lines of approximately the same z-value with different excitation potentials. The abundance for each line was chosen so that each line had the same equivalent width before a magnetic field was applied. Figure 4 shows a plot of the intensification as a function of excitation potential. There is some scatter in the points, but with the exception of the line with excitation potential of 0.11 eV the lines have essentially the same intensification. The line of 0.11 eV is a resonance line and the theory used in this study is questionable for resonance lines (see Appendix B). The fact that the intensification is independent of excitation potential is not surprising, because an intutitive argument leads to the same result.

Boyarchuk, Efimov, and Stepanov (1961) find that the magnetic intensification increases with increasing angle, γ. Figure 5 shows that this is not true in all cases. This figure is for Fe I (152) λ4210.35. The different curves are for different abundances, and therefore they correspond to different points on the curve of growth. The solid curve in the figure for H = 4000 G shows that in some cases the intensification reaches a maximum at a value of γ other than 90°. Figure 5 shows that a de-intensification occurs in the longitudinal effect. This de-intensification seems to be due to a difference in numerical processes used in the calculation of the line profiles when Zeeman broadening is allowed rather than a real physical effect.

Figure 6 shows the intensification as a function of the number of Zeeman components. The five lines used all come from Fe I (152), and all have approximately the same z-value. The abundance for each line was chosen so that each line has the same equivalent width when there is no magnetic field. The solid line in the figure represents the maximum intensification (n/2) that

EXPLANATION OF PLATE IV

Fig. 4. - Magnetic intensification for several different normal triplet lines of Fe I is shown as a function of excitation potential for transverse field of 2000 G. The lines all have approximately the same z-value and the abundance was chosen so that the lines have the same theoretical equivalent width for the zero field calculation.

PLATE IV

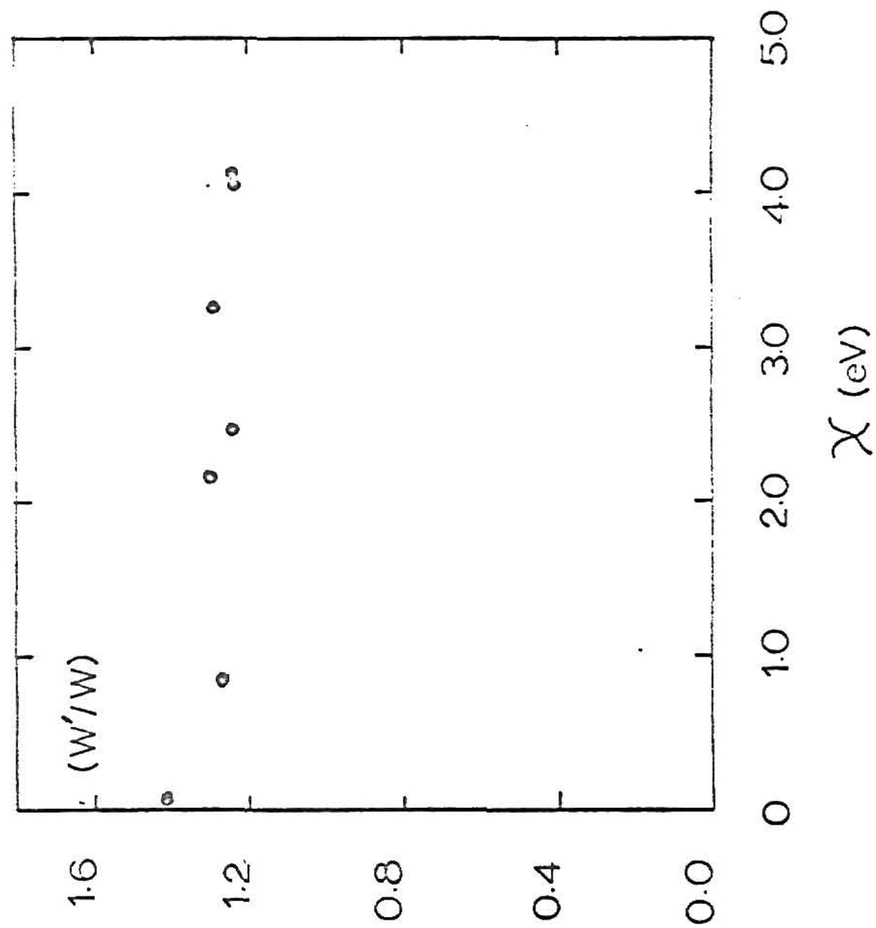

EXPLANATION OF PLATE V

Fig. 5. - Magnetic intensification as a function of γ the angle between the line-of-sight and the magnetic field direction is shown for three different relative abundances. The line is the Fe I λ4210.35 line for a magnetic field strength of 2000 G.

Fig. 6. - The same calculations are shown as in Figure 5 with a field strength of 4000 G.

PLATE V

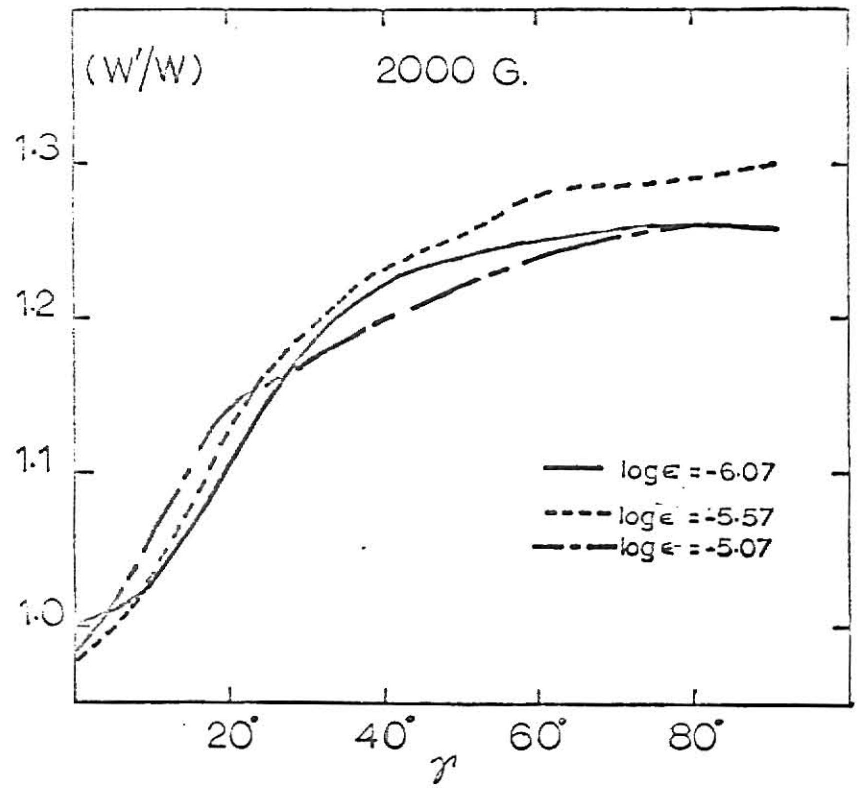
(W′/W)
2000 G.
1·3
1·2
1·1
1·0
log ε = -6·07
log ε = -5·57
log ε = -5·07
20°
40°
60°
80°
γ

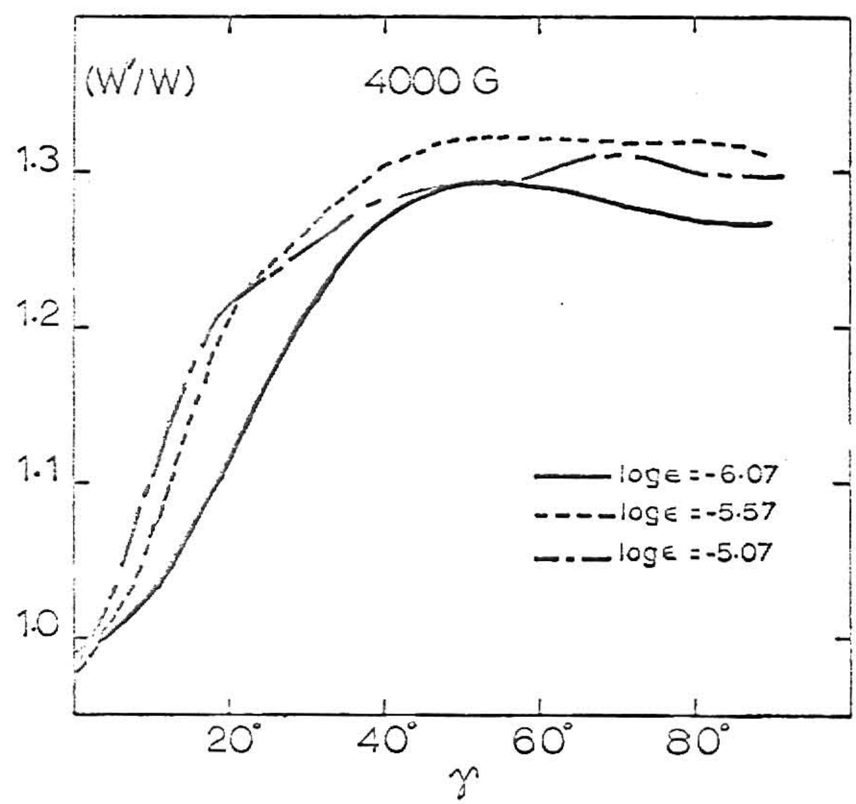
(W′/W)
4000 G
1·3
1·2
1·1
1·0
log ε = -6·07
log ε = -5·57
log ε = -5·07
20°
40°
60°
80°
γ

EXPLANATION OF PLATE VI

Fig. 7. - The magnetic intensification is shown as a function of n, the number of components in the Zeeman pattern, for transverse fields of 2000 G (o) and 4000 G (x).

PLATE VI

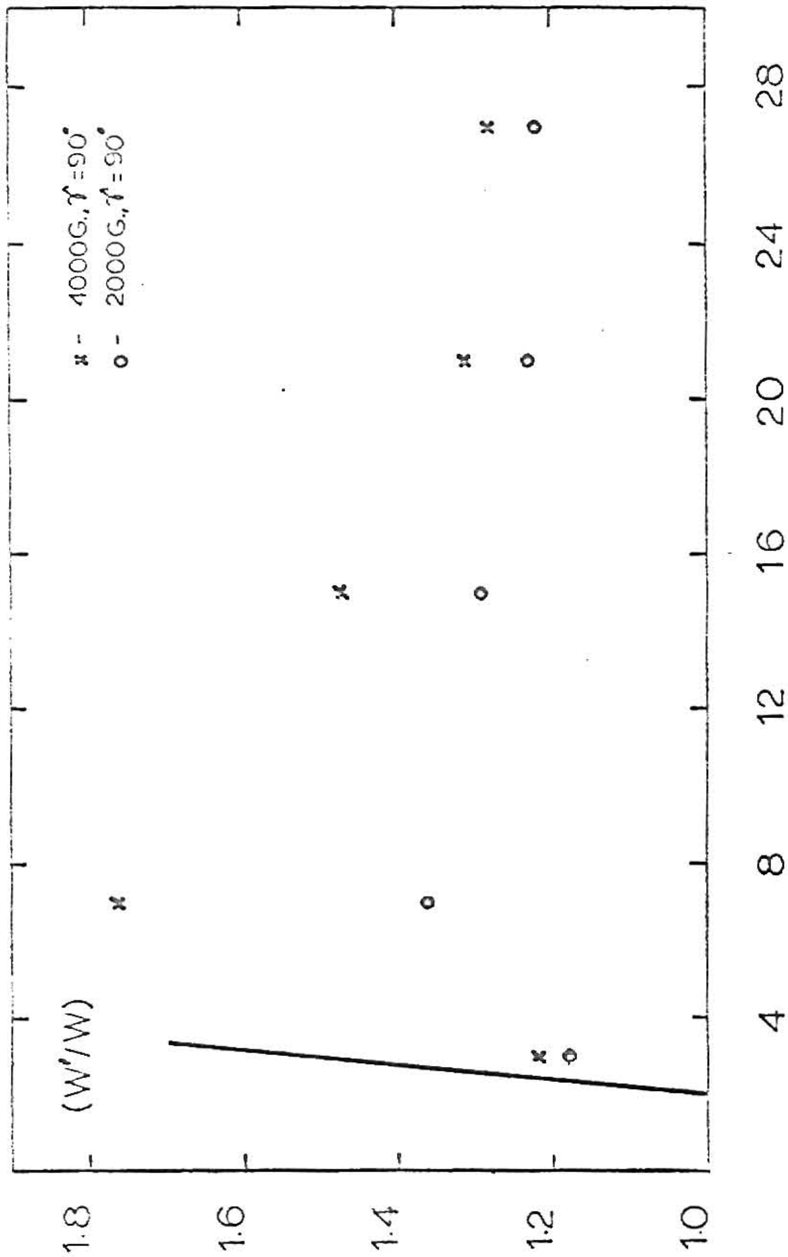

can be attributed to the Zeeman splitting (Babcock 1949). The intensification does not continue to increase as the number of Zeeman components is increased. This is due to the fact that pressure and thermal mechanisms have already broadened the line beyond the width of the Zeeman pattern.

The maximum overabundance that could be attributed to magnetic intensification was estimated for selected lines of C I, Si I, Si II, Fe I, Fe II, and Eu II (see Table 3) for all ten model atmospheres. The results of this investigation are given in Table 4 where the computations were made for the transverse effect with a magnetic field of 2000 G. In cases where more than one line of a given ionization stage were used in the calculations the result given in Table 4 is for the line that exhibited the maximum overabundance. The maximum overabundance varies from a value of 1.2 to 6.6 The magnetic intensification is more important in the heavy elements and does not seem to depend on the ionization stage.

The effect on the maximum overabundance due to increasing the magnetic field strength for model number 8 is given in Table 5. The computations were done for the transverse case. Table 5 shows that overabundance does not increase as the magnetic field is increased for all values of the magnetic field. The value of the magnetic field beyond which an increase in field strength does not result in an increase in overabundance depends on the Zeeman pattern of the line. This does not agree with the results of Boyarchuk, Efimov, and Stepanov (1961). They found the magnetic strengthening to increase with increasing field strength (for all field strengths observed in atmospheres of magnetic stars).

The overabundance estimates that we have obtained are not large enough to explain all of the apparent abundance anomalies that are observed in the

TABLE 4

THE MAXIMUM OVERABUNDANCE DUE TO

MAGNETIC INTENSIFICATION

Model Number	C I	Si I	Si II	Fe I	Fe II	Eu II
1	1.4	1.7	1.3	2.8	3.7	3.5
2	1.5	1.6	1.2	2.1	2.4	2.8
3	1.4	1.6	1.2	2.8	2.9	3.5
4	1.3	1.5	1.2	3.4	3.2	2.9
5	1.4	2.3	1.2	3.3	4.6	4.7
6	1.3	1.7	1.3	3.3	3.2	3.5
7	1.5	1.7	1.4	4.5	5.1	5.5
8	1.2	1.6	1.3	4.6	3.6	4.0
9	1.4	2.1	1.4	6.3	6.3	6.6
10	1.3	1.9	1.3	3.9	5.4	5.5

TABLE 5

MAXIMUM OVERABUNDANCE FOR MODEL NUMBER 8

Magnetic Field (Gauss)	C I	Si I	Si II	Fe I	Fe II	Eu II
2000	1.2	1.6	2.2	4.6	3.6	3.9
4000	1.8	2.0	2.7	5.5	8.3	7.6
6000	2.3	2.8	3.6	5.5	8.7	12.9
8000	2.3	3.3	3.6	5.5	8.7	18.2

Ap stars especially those found for the rare earth elements. Sargent (1966) lists in tabular form the overabundances measured in certain of the peculiar A stars. The overabundances listed for Si range from a factor of 1.3 to about 10. The maximum overabundance for Fe listed in this table is 6.4 and the Eu overabundance ranges from a factor of 100 to 1000. Table 5 shows that the overabundance due to magnetic intensification is large enough to account for some of the anomalous abundances found in the peculiar A stars. The results do show that care should be taken when using a curve of growth analysis to determine abundances in magnetic stars. Figure 2 shows that if a microturbulent velocity is included in the curve of growth analysis the magnetic intensification will have an effect that is much smaller than that found in this study. This is due to the broadening of the line by the microturbulent velocity (see Appendix B).

APPENDIX A

MODEL STELLAR ATMOSPHERE CALCULATIONS

a) Introduction

The atmosphere of a star is defined as those layers from which a photon, emitted in the outward direction, has a high probability of escaping before it can be absorbed. Stellar atmospheres are about 500 to 1000 km in thickness and contain a negligible amount of the mass of the star. Since the radiation that we receive from the star was emitted somewhere in the atmosphere, the character of the radiation is determined by the physical conditions in the atmosphere. The total rate of radiant energy loss by a star is determined by the energy generation processes in the interior, but the frequency distribution is characteristic of the atmosphere.

The model atmosphere approach was developed as the stellar spectroscopist began to try to interpret the observational data he obtained. Since a complete representation of a stellar atmosphere either physically or mathematically is not possible at the present time, certain simplifying assumptions are made in order to construct a model atmosphere. The assumptions used in this study are common to most model atmosphere investigations (See Unsold 1955, Aller 1963, Pecker 1965). Essentially the problem we consider is the modified restricted problem of Milne (Kourganoff 1963) where the assumptions are: (i) the star is spherically-symmetric, non-rotating, and non-magnetic; (ii) the atmosphere is stratified in homogeneous, steady-state, plane-parallel layers and is in hydrostatic equilibrium with no radiation, magnetic, or mechanical forces; (iii) energy is transported by radiation and convection and there are no sources or sinks of energy; (iv) local thermodynamic equilibrium (LTE) is assumed to hold, which is mathematically equivalent to the statement that at each layer in the atmosphere a local electron kinetic temperature can be defined such that the source function is the Planck function; and (v) line and continuum formation can be separated.

The assumption that the atmosphere is non-magnetic seems inconsistent since this study is concerned with the effects of magnetic fields on stellar abundance determinations. However, magnetic forces are not totally neglected in as much as we use an effective surface gravity and not the dynamical surface gravity. The magnetic forces produce a magnetic pressure which acts to distend the atmosphere in opposition to the dynamical surface gravity.

As discussed in Section II, the fact that radiation is taken as the only means of energy transport is based in part on a study by Mihalas (1966). In this article Mihalas states that convection in the hydrogen ionization zone first makes its appearance in the range of spectral type from roughly B8 to FO ($0.45 \lesssim \theta_e \lesssim 0.70$). But he states from a previous study (Mihalas (1965b)) that for $\theta_e \lesssim 0.70$ the presence of the convection has no appreciable effect upon the emitted spectrum in the visible region. A second reason is the theoretical argument that a magnetic field will tend to inhibit convection. This stems from the fact that magnetic lines of force tend to be frozen into a highly conductive medium such as a stellar photosphere as shown by Chandrasekhar (Aller 1963).

In the investigation from which the temperature distributions were taken (see Section II) Mihalas makes the same assumptions as mentioned above.

b) The Pressure-Opacity-Flux Model

It is convenient to use a quantity other than the actual physical depth as the independent depth variable. The quantity found in practice to be most suitable is the logarithm of the continuum optical depth at 5000 Å. This quantity is related to the physical depth scale t by the relation

$$X = \log \tau_0 = \log\left[\int_0^t \frac{\kappa_0(t)\,\rho(t)}{m_0 \sum_i \epsilon_i \mu_i}\, dt\right] \quad , \tag{A1}$$

where κ_0 = the continuous absorption coefficient per hydrogen particle at 5000 Å,

ρ = the density of the stellar material,

μ_i = the atomic weight of species i,

ϵ_i = the ratio of the number density of species i to that of hydrogen,

m_0 = the mass in grams of a unit of atomic weight.

The quantity $1/m_0 \sum_i \epsilon_i \mu_i$ is the number of hydrogen particles per gram of stellar material.

Since we have assumed LTE the ionization equilibrium can be calculated from the Saha equation. The elements considered in the calculation of the ionization equilibrium are listed in Table 1. Only neutral and singly ionized particles are considered in determining the ionization equilibrium, and He ionization and molecular formation are neglected. Mihalas (1965a) allowed He ionization in his study and found that it is negligible over the temperature range covered in this study. The Saha equation for the ratio of single ions to neutral particles of species i is given by (Aller 1963)

$$\frac{n_2}{n_1} = 10^{\log(u_2/u_1) + (9.0801 - 2.5 \log\theta - \log P_e) - \chi_1\theta}$$
$$\equiv \Phi_i / P_e \quad , \tag{A2}$$

where n_2 = number density of singly ionized particles of species i,

n_1 = number density of neutral particles of species i,

χ_1 = ionization potential between the neutral and singly ionized stage in eV,

U_1 = partition function for neutral particles of species i,

U_2 = partition function for singly ionized particles of species i,

θ = 5040/T,

P_e = the electron pressure.

Now the ratio of ions to atoms plus ions can be written as

$$\left[\frac{n_2}{n_1+n_2}\right]_i = \frac{\Phi_i/P_e}{1+(\Phi_i/P_e)} \equiv X_i \quad . \tag{A3}$$

Since we assume only one stage of ionization, the number of free electrons is equal to the number of ions. Then the ratio of all atoms, ions, and electrons to electrons is given by

$$\frac{N}{N_e} = \frac{n_{He} + \sum_i (n_1+n_2+n_e)}{\sum_i (n_e)_i} \quad . \tag{A4}$$

If we divide numerator and denominator by the number density of hydrogen particles, N_H, introduce ϵ_i, and use the perfect gas law to convert to a ratio of pressures, the proceeding equation then becomes

$$\frac{P_g}{P_e^2} = \frac{\epsilon_{He} + \sum_i \epsilon_i (1+X_i)}{P_e \sum_i \epsilon_i X_i} \quad , \tag{A5}$$

where we have divided both sides of the equation by P_e. The reason for dividing by P_e is that the function P_g/P_e^2 has been found to be less sensitive to P_e than to θ (Weidemann 1955) which is important in the actual computations.

The sources of continuous opacity has previously been discussed in Section II. Because of its high abundance, hydrogen is the primary contributor in the form of H and H^-. This is especially true for the visible spectrum.

In the near ultraviolet, H_2^+ and the collective contributions of several metals are also significant contributors. We have neglected molecular and negative ion absorption from other elements because of their low abundances. The metallic absorption was treated with a hydrogen-like approximation and integrated over the absorption edges. The scattering contributions considered are: (i) Rayleigh scattering by neutral hydrogen; and (ii) Thompson scattering by free electrons. A general discussion of the calculation of continuous absorption coefficients and scattering contributions is given by Unsold (1955), Aller (1963), Gingerich (1964) and Mihalas (1967). A description of the exact methods employed in this study is given by Evans (1966).

The depth-dependent total monochromatic absorption coefficient per hydrogen particle can be written in the form

$$\frac{K_\lambda}{P_e} = \left[\frac{K_\lambda(H)}{P_e} + \frac{K_\lambda(M)}{P_e} \right] (1-10^{-\chi_\lambda \theta}) + \frac{\sigma}{P_e} , \tag{A6}$$

where $K_\lambda(H)$ = the bound-free and free-free contribution from hydrogen in the form H, H^-, H_2^+,

$K_\lambda(M)$ = the bound-free and free-free contribution from the metals,

σ = the scattering coefficient per hydrogen particle,

$(1-10^{-\chi_\lambda \theta})$ = the correction for stimulated emissions,

$\chi_\lambda = 12397.67/\lambda$.

Since we use the logarithm of the optical depth at 5000 Å as our independent depth variable we must use K_λ/P_e at $\lambda = 5000$ Å in computing the pressure model.

The final equation needed to compute the pressure model is the equation of hydrostatic equilibrium (Aller 1963). We can write this equation in terms of the continuous absorption coefficient at 5000 Å, the effective surface gravity, and then convert to a logarithmic optical depth scale. If the equation is then multiplied by $P_g^{1/2}$ and integrated from the top of the atmosphere, where $P_g = 0$, to the depth x, the resulting integral equation (Evans 1966) is

$$\log P_g = \frac{2}{3}\left[\log C_{P_g} + \log\left[\int_{-\infty}^{x}\left[\frac{P_g}{P_e^2}\right]\frac{\tau_o}{(\kappa_o/P_e)}\,dx\right]\right] , \tag{A7}$$

where $C_{P_g} = 3/2\ (gm_o \sum_i \epsilon_i \mu_i/\mathrm{Mod})$,

g = effective surface gravity,

Mod = 0.4343.

Since the pressure model computation is an iteration on the electron pressure, the electron pressure is obtained from P_g and P_g/P_e^2 by the equation

$$\log P_e = \frac{1}{2}\left[\log P_g - \log(P_g/P_e^2)\right] . \tag{A8}$$

For a steady-state, plane-parallel stellar atmosphere Aller (1963) gives the solution to the equation of radiative transfer for the surface flux in the form

$$F_\lambda(0) = 2\int_0^{+\infty} B_\lambda(\tau_\lambda)\, E_2(\tau_\lambda)\, d\tau_\lambda , \tag{A9}$$

where the previous assumption of LTE gives the Planck function $B_\lambda(\tau_\lambda)$ as the source function, E_2 is the second exponential integral given by

$$E_2(x) = \int_{-\infty}^{x} \frac{e^{-x\omega}}{\omega^2}\, d\omega , \tag{A10}$$

and the optical depth at the wavelength λ is computed for given values of the independent variable x by the equation

$$\tau_\lambda(x) = \int_{-\infty}^{x} \frac{\kappa_\lambda(x)}{\kappa_o(x)}\left[\frac{\tau_o}{\mathrm{Mod}}\right] dx . \tag{A11}$$

It should be mentioned that the actual physical flux is given by $\pi F_\lambda(0)$.

c) The Computational Procedure

The equations in the preceding section were programed for a digital computer by Elste and later modified by Evans (1969). The input parameters for the computation are: (i) the temperature distribution; (ii) effective surface gravity; (iii) chemical composition; and (iv) an initial estimate of the electron pressure. Using the initial electron pressure, the value of P_g/P_e^2 is calculated from equation (A5) for the assumed chemical composition and temperature distribution. Then the temperature distribution and initial electron pressure are used in equation (A6) to determine K_o/P_e. This value along with the chemical composition, logarithm of the effective surface gravity, and the previously computed quantity P_g/P_e^2 are used in equation (A7) to calculate an initial estimate of the gas pressure P_g. Next from equation (A8) log P_g and P_g/P_e^2 are used to compute a new estimate for the electron pressure. This procedure is then repeated until it converges to a consistent value for the electron pressure. For the opacity model, the absorption coefficient for wavelengths other than 5000 Å is computed from (A6), and the optical depth for these wavelengths is computed by integrating equation (A11). Finally the emitted flux is obtained from the same wavelengths as the opacity model by integrating equation (A9). The opacity-flux model was obtained for wavelengths between 2000 and 10000 Å at intervals of about 300 Å for use in computing the line spectrum.

The details of the model atmospheres used in this study are given in Tables A1, A2, A3, A4, and A5. Other characteristics of these models were previously given in Table 2. Figure A1 shows a comparison of the predicted flux from model 4 to the continuous energy distribution for the Ap star 52 Her measured by Baschek and Oke (1965). They made the measurements using the 100-inch telescope at Mt. Wilson. Finally Figures A2 and A3 compare the measured profiles of H_{β} and H_{γ} for 52 Her and those from model 4. The purpose of these two plates is to show that the models that have been computed are satisfactory representations of stellar atmospheres and particularly the Ap stars.

TABLE A1

AO MODEL ATMOSPHERES

	log g = 4.0				log g = 3.5			
$\log \tau_o$	θ	$\log P_e$	$\log P_g$	$\log K_o/P_e$	θ	$\log P_e$	$\log P_g$	$\log K_o/P_e$
-4.00	0.672	0.549	1.302	-24.799	0.672	0.231	0.812	-24.485
-3.80	.672	0.481	1.194	-24.732	.672	0.156	0.705	-24.406
-3.60	.672	0.549	1.302	-24.799	.672	0.231	0.812	-24.485
-3.40	.672	0.629	1.433	-24.876	.672	0.319	0.942	-24.577
-3.20	.672	0.721	1.581	-24.957	.672	0.421	1.091	-24.676
-3.00	.670	0.825	1.738	-25.034	.670	0.535	1.253	-24.772
-2.80	.668	0.930	1.899	-25.107	.668	0.650	1.420	-24.865
-2.60	.666	1.035	2.062	-25.176	.666	0.764	1.590	-24.953
-2.40	.664	1.139	2.225	-25.240	.664	0.877	1.760	-25.034
-2.20	.661	1.247	2.385	-25.296	.661	0.994	1.929	-25.107
-2.00	.665	1.371	2.536	-25.339	.655	1.123	2.087	-25.162
-1.80	.650	1.484	2.681	-25.380	.650	1.242	2.238	-25.214
-1.60	.640	1.626	2.814	-25.405	.640	1.386	2.377	-25.245
-1.40	.628	1.775	2.933	-25.421	.628	1.536	2.500	-25.263
-1.20	.612	1.943	3.035	-25.422	.612	1.701	2.606	-25.262
-1.00	.595	2.109	3.124	-25.414	.595	1.863	2.697	-25.251
-0.80	.570	2.316	3.196	-25.375	.570	2.058	2.771	-25.209
-0.60	.548	2.488	3.254	-25.336	.548	2.217	2.831	-25.172
-0.40	.519	2.680	3.301	-25.274	.519	2.384	2.884	-25.125
-0.20	.491	2.835	3.341	-25.225	.491	2.512	2.933	-25.109
0.00	.460	2.961	3.380	-25.207	.460	2.617	2.986	-25.137
0.20	.430	3.052	3.424	-25.241	.430	2.706	3.053	-25.206
0.40	.403	3.131	3.482	-25.308	.403	2.800	3.139	-25.290
0.60	.376	3.221	3.561	-25.407	.376	2.911	3.246	-25.396
0.80	.351	3.326	3.662	-25.502	.351	3.038	3.372	-25.495
1.00	.329	3.445	3.780	-25.585	.329	3.172	3.506	-25.495
1.20	0.310	3.548	3.882	-25.654	0.310	3.289	3.622	-25.650

TABLE A2

A2 MODEL ATMOSPHERES

		log g = 4.0				log g = 3.5		
log τ_o	θ	log P_e	log P_g	log K_o/P_e	θ	log P_e	log P_g	log K_o/P_e
-4.00	0.722	0.343	1.497	-25.032	0.722	0.048	0.968	-24.708
-3.80	.722	0.343	1.497	-25.032	.722	0.048	0.968	-24.708
-3.60	.721	0.425	1.638	-25.102	.721	0.136	1.111	-24.803
-3.40	.721	0.508	1.793	-25.174	.721	0.228	1.275	-24.906
-3.20	.721	0.595	1.957	-25.242	.721	0.325	1.453	-25.007
-3.00	.721	0.683	2.126	-25.304	.721	0.426	1.638	-25.103
-2.80	.720	0.778	2.294	-25.358	.720	0.532	1.824	-25.186
-2.60	.718	0.877	2.456	-25.403	.718	0.641	2.004	-25.256
-2.40	.716	0.972	2.614	-25.442	.716	0.746	2.176	-25.316
-2.20	.712	1.079	2.764	-25.475	.712	0.860	2.339	-25.364
-2.00	.709	1.175	2.908	-25.504	.709	0.962	2.495	-25.407
-1.80	.704	1.283	3.048	-25.530	.704	1.075	2.643	-25.442
-1.60	.696	1.409	3.178	-25.553	.696	1.205	2.781	-25.471
-1.40	.686	1.545	3.299	-25.575	.686	1.343	2.906	-25.494
-1.20	.674	1.691	3.411	-25.594	.674	1.490	3.021	-25.513
-1.00	.656	1.875	3.509	-25.609	.656	1.674	3.121	-25.522
-0.80	.632	2.094	3.591	-25.614	.632	1.891	3.202	-25.513
-0.60	.607	2.312	3.657	-25.605	.607	2.103	3.266	-25.489
-0.40	.574	2.575	3.707	-25.566	.574	2.357	3.314	-25.430
-0.20	.540	2.828	3.742	-25.500	.540	2.593	3.347	-25.351
0.00	.501	3.083	3.766	-25.404	.501	2.816	3.370	-25.257
0.20	.465	3.271	3.783	-25.327	.465	2.961	3.390	-25.213
0.40	.434	3.383	3.799	-25.304	.434	3.041	3.412	-25.235
0.60	.402	3.455	3.820	-25.340	.402	3.099	3.444	-25.309
0.80	.375	3.506	3.852	-25.423	.375	3.158	3.494	-25.408
1.00	.350	3.563	3.901	-25.511	.350	3.234	3.568	-25.503
1.20	0.330	3.609	3.941	-25.584	.330	3.296	3.627	-25.578

TABLE A3

A4 MODEL ATMOSPHERES

	log g = 4.0				log g = 3.5			
log τ_o	θ	log P_e	log P_g	log K_o/P_e	θ	log P_e	log P_g	log K_o/P_e
-4.00	0.770	0.303	2.065	-25.320	0.770	0.089	1.649	-25.173
-3.80	.769	0.246	1.954	-25.381	.769	0.035	1.545	-25.173
-3.60	.769	0.303	2.065	-25.316	.769	0.089	1.649	-25.166
-3.40	.769	0.368	2.192	-25.351	.769	0.153	1.773	-25.217
-3.20	.769	0.428	2.329	-25.383	.769	0.225	1.913	-25.268
-3.00	.769	0.511	2.473	-25.412	.769	0.302	2.063	-25.315
-2.80	.768	0.589	2.618	-25.437	.768	0.384	2.217	-25.357
-2.60	.767	0.670	2.763	-25.459	.767	0.470	2.371	-25.392
-2.40	.767	0.747	2.907	-25.478	.767	0.552	2.523	-25.422
-2.20	.765	0.834	3.049	-25.495	.765	0.642	2.673	-25.448
-2.00	.762	0.926	3.187	-25.511	.762	0.738	2.817	-25.471
-1.80	.758	1.023	3.320	-25.527	.758	0.837	2.955	-25.491
-1.60	.753	1.125	3.449	-25.543	.753	0.942	3.088	-25.511
-1.40	.744	1.253	3.571	-25.563	.744	1.072	3.213	-25.533
-1.20	.736	1.372	3.688	-25.581	.736	0.191	3.332	-25.552
-1.00	.718	1.559	3.793	-25.612	.718	1.379	3.439	-25.580
-0.80	.700	1.740	3.887	-25.640	.700	1.560	3.533	-25.604
-0.60	.671	1.997	3.966	-25.675	.671	1.816	3.611	-25.628
-0.40	.637	2.282	4.028	-25.699	.637	2.098	3.670	-25.634
-0.20	.595	2.617	4.071	-25.696	.595	2.427	3.710	-25.603
0.00	.553	2.938	4.099	-25.649	.553	2.737	3.736	-25.530
0.20	.508	3.256	4.117	-25.555	.508	3.034	3.751	-25.417
0.40	.469	3.495	4.127	-25.458	.469	3.238	3.761	-25.328
0.60	.431	3.667	4.136	-25.388	.431	3.367	3.770	-25.299
0.80	.398	3.756	4.145	-25.391	.398	3.428	3.782	-25.341
1.00	.372	3.799	4.158	-25.452	.372	3.463	3.801	-25.431
1.20	0.350	3.836	4.170	-25.521	0.350	3.493	3.818	-25.510

TABLE A4

A7 MODEL ATMOSPHERES

	log g = 4.0				log g = 3.5			
log τ_o	θ	log P_e	log P_g	log K_o/P_e	θ	log P_e	log P_g	log K_o/P_e
-4.00	0.826	0.158	1.977	-25.272	0.826	0.399	1.504	-25.115
-3.80	.825	0.078	2.131	-25.307	.825	0.309	1.679	-25.184
-3.60	.825	0.000	2.284	-25.335	.825	0.218	1.854	-25.240
-3.40	.825	0.079	2.436	-25.358	.825	0.130	2.024	-25.284
-3.20	.825	0.156	2.584	-25.376	.825	0.044	2.189	-25.319
-3.00	.825	0.232	2.730	-25.390	.825	0.037	2.348	-25.346
-2.80	.824	0.306	2.874	-25.402	.824	0.117	2.502	-25.367
-2.60	.824	0.384	3.015	-25.412	.824	0.199	2.651	-25.384
-2.40	.823	0.462	3.154	-25.421	.823	0.280	2.796	-25.393
-2.20	.822	0.539	3.291	-25.429	.822	0.359	2.938	-25.410
-2.00	.820	0.622	3.425	-25.438	.820	0.444	3.076	-25.422
-1.80	.817	0.711	3.557	-25.447	.817	0.534	3.211	-25.434
-1.60	.812	0.813	3.684	-25.460	.812	0.637	3.341	-25.448
-1.40	.804	0.933	3.806	-25.478	.804	0.758	3.464	-25.466
-1.20	.793	1.071	3.920	-25.500	.793	0.897	3.580	-25.489
-1.00	.778	1.234	4.026	-25.530	.778	1.061	3.686	-25.518
-0.80	.760	1.415	4.122	-25.564	.760	1.243	3.782	-25.551
-0.60	.732	1.664	4.206	-25.615	.732	1.492	3.865	-25.598
-0.40	.699	1.944	4.274	-25.669	.699	1.771	3.933	-25.645
-0.20	.660	2.263	4.327	-25.722	.660	2.088	3.985	-25.685
0.00	.611	2.649	4.365	-25.758	.611	2.472	4.020	-25.644
0.20	.558	3.055	4.388	-25.738	.558	2.870	4.041	-25.640
0.40	.510	3.406	4.401	-25.661	.510	3.205	4.052	-25.536
0.60	.463	3.712	4.409	-25.547	.463	3.477	4.058	-25.417
0.80	.425	3.902	4.414	-25.463	.425	3.623	4.063	-25.361
1.00	.393	4.002	4.419	-25.445	.393	3.689	4.069	-25.388
1.20	0.365	4.090	4.423	-25.497	0.365	3.246	4.074	-25.468

TABLE A5

F0 MODEL ATMOSPHERES

	log g = 4.0				log g = 3.5			
log τ_o	θ	log P_e	log P_g	log K_o/P_e	θ	log P_e	log P_g	log K_o/P_e
-4.00	0.886	-0.285	2.580	-25.279	0.886	-0.465	2.228	-25.242
-3.80	.886	-0.352	2.450	-25.268	.886	-0.530	2.102	-25.223
-3.60	.886	-0.285	2.580	-25.279	.886	-0.465	2.228	-25.242
-3.40	.885	-0.210	2.712	-25.290	.885	-0.391	2.360	-25.260
-3.20	.885	-0.141	2.845	-25.298	.885	-0.322	2.495	-25.274
-3.00	.884	-0.065	2.979	-25.307	.884	-0.245	2.631	-25.387
-2.80	.884	0.004	3.114	-25.312	.884	-0.174	2.768	-25.296
-2.60	.883	0.080	3.247	-25.319	.883	-0.097	2.904	-25.305
-2.40	.883	0.150	3.381	-25.323	.883	-0.027	3.040	-25.311
-2.20	.882	0.227	3.513	-25.328	.882	0.049	3.174	-25.318
-2.00	.881	0.304	3.645	-25.333	.881	0.126	3.308	-25.324
-1.80	.877	0.400	3.774	-25.343	.877	0.223	3.429	-25.335
-1.60	.872	0.501	3.898	-25.354	.872	0.324	3.565	-25.348
-1.40	.864	0.619	4.018	-25.371	.864	0.443	3.685	-25.365
-1.20	.854	0.749	4.132	-25.391	.854	0.573	3.800	-25.386
-1.00	.838	0.915	4.238	-25.423	.838	0.741	3.906	-25.418
-0.80	.816	1.119	4.332	-25.466	.816	0.947	4.001	-25.460
-0.60	.793	1.327	4.417	-25.510	.793	1.156	4.085	-25.504
-0.40	.756	1.631	4.488	-25.581	.756	1.461	4.155	-25.572
-0.20	.721	1.918	4.545	-25.646	.721	1.749	4.211	-25.633
0.00	.668	2.335	4.588	-25.732	.668	2.165	4.253	-25.707
0.20	.613	2.763	4.617	-25.793	.613	2.591	4.280	-25.743
0.40	.556	3.199	4.634	-25.796	.556	3.021	4.295	-25.711
0.60	.501	3.603	4.643	-25.721	.501	3.411	4.303	-25.606
0.80	.454	3.910	4.648	-25.597	.454	3.695	4.307	-25.490
1.00	.417	4.087	4.651	-25.494	.417	3.858	4.310	-25.430
1.20	0.390	4.216	4.653	-25.481	0.390	3.976	4.312	-25.445

EXPLANATION OF PLATE VII

Fig. A1. - A comparison is shown of the observed relative continuous energy distribution for 52 Her and that predicted for model 4 on a magnitude scale in frequency units.

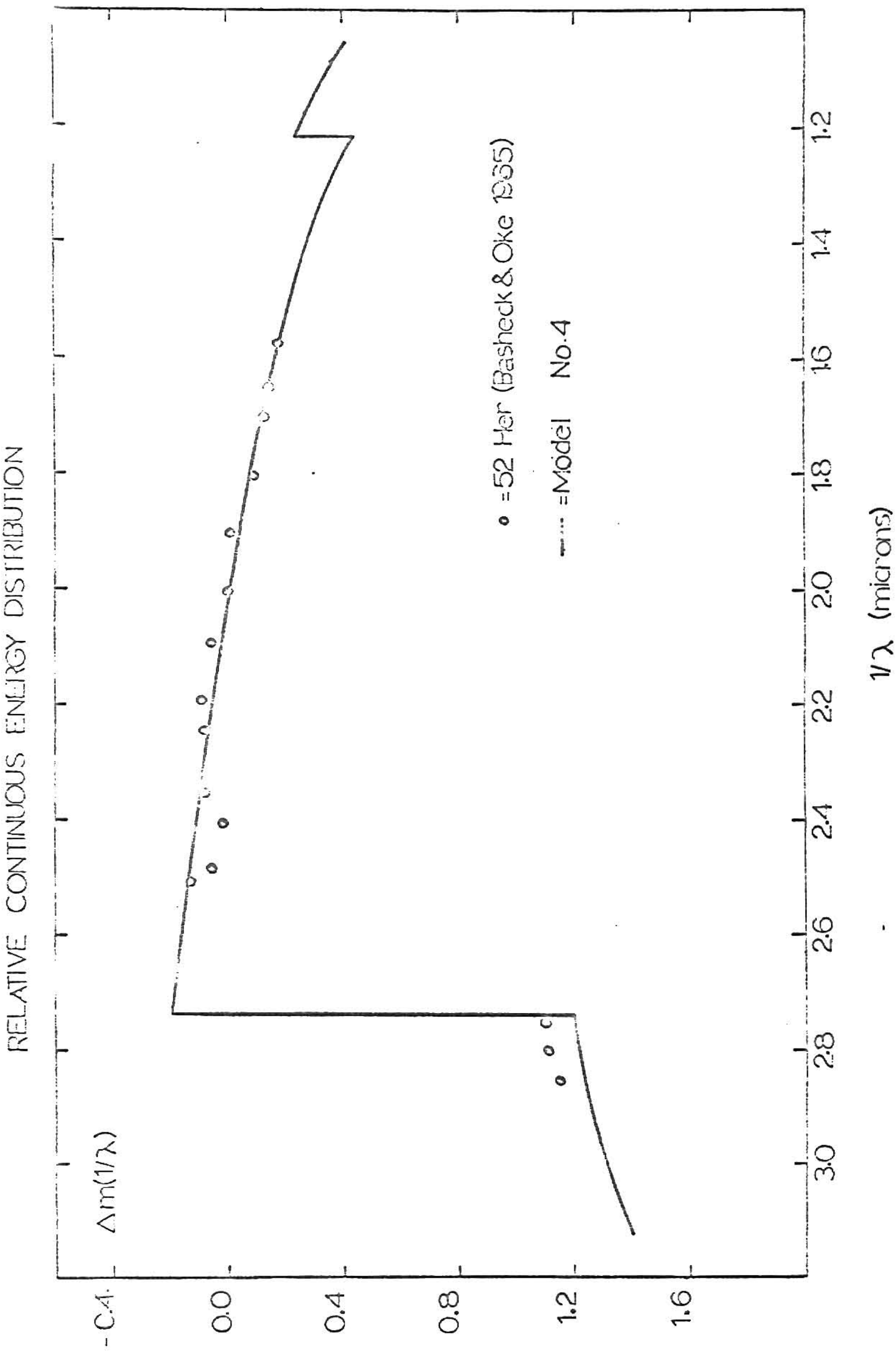
RELATIVE CONTINUOUS ENERGY DISTRIBUTION
o =52 Her (Basheck & Oke
=Model No.4
Δm(1/λ)
-0.4
0.0
0.4
0.8
1.2
1.6
3.0
2.8
2.6
2.4
2.2
2.0
1.8
1.6
1.4
1.2
1/λ (microns)

EXPLANATION OF PLATE VIII

Fig. A2. - A comparison is shown of the observed line profiles for H_β for 52 Her and that calculated for model 4.

Fig. A3. - The same comparison as in the proceeding figure for the H_γ line.

PLATE VIII

MODEL No. 4

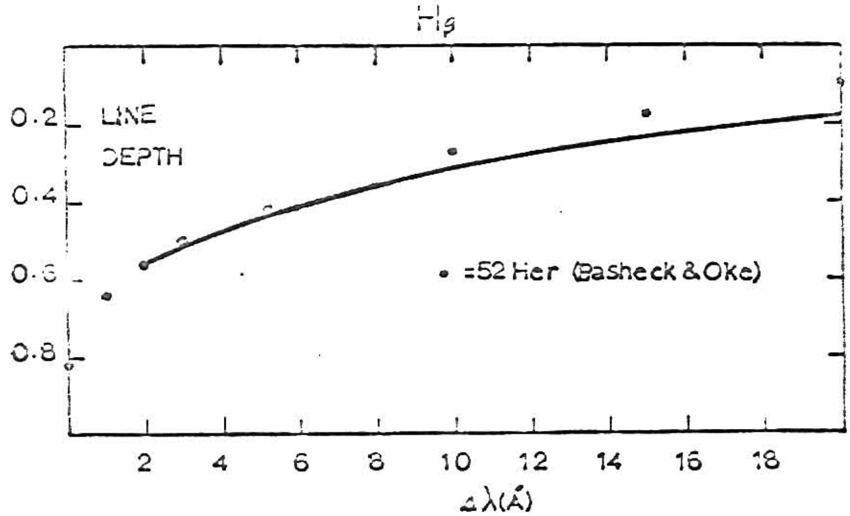

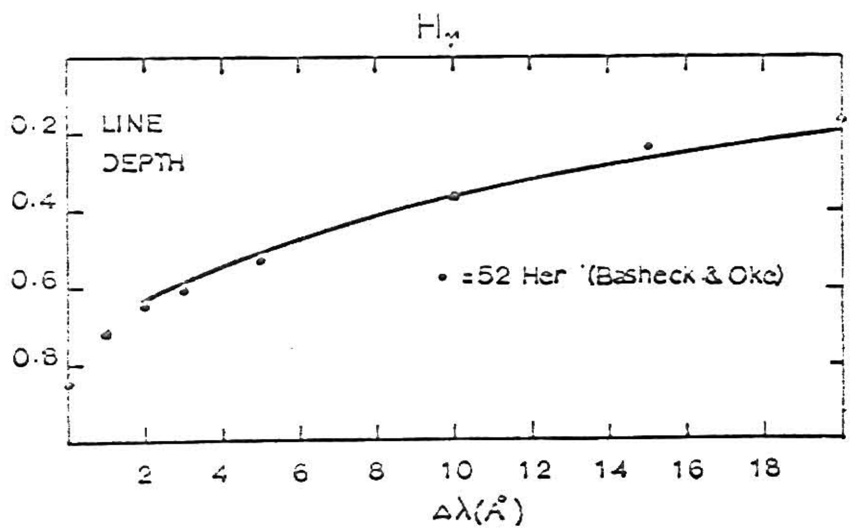

APPENDIX B

STELLAR ABSORPTION LINE CALCULATIONS

a) The Theoretical Line Profile

In this investigation the absorption lines are assumed to be formed in LTE; therefore, the source function is the Planck function. This assumption is more valid for subordinate transitions, which tend to favor pure absorption, than for resonance transitions (Aller 1963).

The line depth in flux is defined as

$$R = \frac{F_\lambda(0) - F_{\Delta\lambda}(0)}{F_\lambda(0)} \quad , \tag{B1}$$

where $F_\lambda(0)$ = the emergent continuum flux,

$F_{\Delta\lambda}(0)$ = the emergent flux in the line at the point $\Delta\lambda$ from the line center.

The quantity $F_\lambda(0)$ is obtained from the model atmosphere calculation. Since the continuum flux is not a strongly varying function of wavelength except in the neighborhood of an absorption discontinuity, sufficient accuracy is obtained by using the continuum flux in a wavelength interval of $\lambda\lambda$100-200 containing the line of interest. Therefore, in order to calculate the line depth the quantity $F_{\Delta\lambda}(0)$ must be determined. Gussman (1967) proposed a gradient method which has been modified by Evans (1969) and was used in calculating the line depth

$$R = \int_{-\infty}^{+\infty} \frac{2}{F_\lambda(0)} \left[\frac{dB_\lambda}{dx}\right] E_3(\tau_\lambda) \left[1 - \frac{E_3(\tau_\lambda + \tau_\ell)}{E_3(\tau_\lambda)}\right] dx \quad , \tag{B2}$$

where $\tau_\ell(x,\Delta\lambda)$ is the optical depth in the line. The optical depth in the line is obtained from the definition of optical depth (equation (A1)) in the form

$$\tau_\lambda(x,\Delta\lambda) = \int_{-\infty}^{x} \frac{K_\ell}{K_o} \left[\frac{\tau_o}{M\,\mathrm{mod}}\right] dx \, , \tag{B3}$$

where $K_\lambda(x,\Delta\lambda)$ is the line absorption coefficient per hydrogen particle, and where $K_o(x)$ and $\tau_o(x)$ are obtained from the model atmosphere calculations. Thus the problem of calculating the line depth reduces to the specification of the absorption coefficient in the line and its variation with $\Delta\lambda$. The line absorption coefficient per hydrogen particle is given by (See Unsold 1955 or Aller 1963)

$$K_\lambda(x,\Delta\lambda) = \left[1-10^{-\chi_\lambda\theta}\right] \frac{N}{N_H} \frac{\sqrt{\pi}\, e^2}{m c^2} \frac{\lambda^2}{\Delta\lambda_D} f \phi_{\Delta\lambda} \quad , \tag{B4}$$

where $(1-10^{-\chi_\lambda\theta})$ = the correction for stimulated emissions,

N = number of absorbing particles in the lower level of the transition of interest per unit volume,

N_H = number of hydrogen particles per unit volume,

$\Delta\lambda_D$ = the Doppler width

$= \frac{\lambda}{c}\sqrt{\xi_{th}^2 + \xi_t^2} \equiv \frac{\lambda}{c}\sqrt{\cdots}$,

ξ_{th} = the most probable thermal velocity of element i,

$= 2RT/\mu_i = 83.83/\mu_i\theta$,

ξ_t = the most probable microturbulent velocity,

f = the oscillator strength,

$\phi_{\Delta\lambda}$ = the broadening function,

and π, e, m, c have their usual meaning. Following the procedure suggested by Evans (1970), the number of absorbing particles per unit volume, N, is obtained from a system of Saha and Boltzmann equations in the form

$$N = \left[\frac{n_{p,s}}{n_p}\right] \left[\frac{n_p}{\sum n_\delta}\right] N_i \tag{B5}$$

where $n_{p,s}$ = the number density of particles in the p-th ionization stage and the s-th excitation state,

and the summation over q represents the summation over all ionization stages and is just equal to N_i.

Let r be the most abundant ionization stage for the temperature and pressure of interest, r-1 the stage below r, r+1 the stage above r. In this study only these three stages of ionization will be considered in the summation over q. Then we can write (Evans 1966)

$$\left[\frac{n_{p,s}}{n_p}\right]\left[\frac{n_p}{\sum n_q}\right] = \left[\frac{n_{p,s}}{n_p}\right]\left[\frac{n_p}{n_{r-1} + n_r + n_{r+1}}\right] = \left[\frac{n_{p,s}\,U_r}{n_r}\right]\left[\frac{1}{\mathcal{U}}\right] , \tag{B6}$$

where U_r = the partition function of the r-th stage of ionization,

$$\mathcal{U} = U_r\left[\frac{n_{r-1}}{n_r} + 1 + \frac{n_{r+1}}{n_r}\right] .$$

The first quantity in equation (B6) can be obtained from the combined Boltzmann and Saha equations. It depends upon which ionization stage is under consideration, and is given in the form (Evans 1966)

$$\log\left[\frac{n_{p,s}\,U_r}{n_r}\right] = \log g_{p,s} + \Delta\chi\theta + h(9.0301 - 2.5\log\theta - \log P_e) \tag{B7}$$

where $g_{p,s}$ = statistical weight of the lower level,

and if $p = r-1$, then $h = -1$ and $\Delta\chi = \chi_{r-1} - \chi_{r-1,s}$

if $p = r$, then $h = 0$ and $\Delta\chi = -\chi_{r,s}$

if $p = r+1$, then $h = +1$ and $\Delta\chi = -\chi_{r+1,s} - \chi_r$

where $\chi_{r,s}$ = the excitation potential in eV.

The absorption coefficient per hydrogen particle can now be written as

$$K_\ell = \epsilon_i \frac{\sqrt{\pi}\,e^2}{mc^2}\,\frac{\lambda^2}{\Delta\lambda_D}\,\frac{g_{p,s}}{\mathcal{U}}\left[10^{\Delta\chi\theta + h(9.0301 - 2.5\log\theta - \log P_e)}\right] \left[1 - 10^{-\chi_\lambda\theta}\right] f\,\phi_{\Delta\lambda} . \tag{B8}$$

The integrand for the line optical depth (see equation (B3)) is written by Evans in the form

$$\frac{K_\ell}{K_o}\left[\frac{\tau_o}{\mathrm{Mod}}\right] = \epsilon_i\,(gf\lambda)_i\,Z_i\,\phi_{\Delta\lambda} \quad , \tag{B9}$$

where Z_i is a depth dependent population factor and ϵ_i is the relative abundance of the species i and the broadening function, $\phi_{\Delta\lambda}$, for metal lines and hydrogen lines will be discussed in Sections c) and d), respectively.

b) Line Broadening

The essential spectroscopic data needed for an investigation of a stellar atmosphere are the continuous energy distribution and the equivalent widths, profiles, and displacements of spectral lines. In order to interpret line profiles and equivalent widths it is necessary to know the nature of the line broadening. For this reason we must consider sources of line broadening and their influence on the absorption coefficient.

Absorption lines in stellar spectra are intrinsically broadened by the following causes (see Aller 1963): (i) a Doppler effect arising from the random thermal motion of the gas atoms and a possible turbulence broadening cuased by mass motion in the atmosphere; (ii) radiation damping or natural broadening, due to the finite lifetimes of excited levels; (iii) resonance broadening, due to collisions of the absorbing atom with atoms of the same kind; (iv) isotopic broadening, a pseudo-broadening due to isotopic differences; (v) Stark broadening, due to interactions of the absorbing atom with ions and electrons; (vi) van der Waals broadening, due to the interaction with neutral atoms or molecules of a different kind than the absorber; (vii) Zeeman broadening, due to Zeeman splitting by a magnetic field. There are also extrinsic causes for broad lines in stellar spectra, such as rotational broadening, which is due to the contributions from different parts of a rotating stellar surface.

It is useful to divide the turbulence broadening into two categories, macroturbulence and microturbulence. Macroturbulence is defined as mass motions of turbulent elements whose linear extent is large compared to the mean free path of a photon, and microturbulence is defined as the mass motions of turbulent elements whose linear extent is small compared to the mean free path of a photon.

Macroturbulence and rotational broadening do not affect the equivalent width of a line, since they take place after the line is formed. However, they will affect the shape of the line. Microturbulence increases the equivalent width of the line by delaying saturation and raising the flat portion of the curve of growth. The broadening mechanisms included in this study are random thermal motions, natural broadening, quadratic Stark effect due to electrons and ions, van der Waals interactions with hydrogen and helium, and Zeeman broadening.

c) The Metal Line Broadening Function

The metal line absorption coefficient is a bound-bound absorption coefficient which depends on the abundance of the absorbing element, the fraction of atoms in the lower level, the relevant transition probability, and the broadening function. It is because of this broadening that lines have a finite width.

The metal line broadening function results from a convolution of a Gaussian (Doppler broadening) with a Lorentz (natural and pressure broadening) profile resulting in a Voigt profile H. Therefore, the metal line broadening function can be written as

$$\Phi_{\Delta\lambda} = H(a, v) \quad , \tag{B10}$$

$$\text{where}\quad H(a,v) = \frac{a}{\pi}\int_{-\infty}^{+\infty}\frac{e^{-y^2}}{(v-y)^2+a^2}\,dy \;,$$

$$v(x) = \Delta\lambda/\Delta\lambda_D \;,$$

$$a(x) = \frac{\Gamma}{4\pi}\;\frac{\lambda}{\sqrt{\xi_{th}^2+\xi_t^2}} \;,$$

$$\Gamma(x) = \Gamma_R + \Gamma_S + \Gamma_W \;.$$

The damping constants were briefly disucssed in Section III. A more detailed discussion is given by Aller (1963, Chap. 7) or for the exact formulation used see Evans (1966).

It the line is formed in the presence of a homogeneous magnetic field the broadening function becomes that $\psi_{\pm}$ discussed in Section III with each Zeeman component being broadened independently by the other broadening mechanisms.

d) The Hydrogen Line Broadening Function

Hydrogen, the simplest atom, has one of the most complicated types of broadening. The reason is that outside the narrow Doppler core the broadening arises from perturbations produced by ions which broaden according to the statistical theory and electrons which broaden according to the impact (discrete encounter) theory (Aller 1963). The slowly varying ion fields split the degenerate hydrogen levels into their component Stark substates which are individually broadened by electron encounters.

In this investigation the hydrogen line calculations were not of paramount importance. Therefore, we shall only briefly outline the essence of the consideration. The hydrogen broadening function is given as the sum of two terms (Underhill and Waddell 1959)

$$f\phi_{\Delta\lambda} = f_o H(a,v) + \frac{\sqrt{\pi}\,\Delta\lambda_D}{F_o}\, f_{\pm}\, I(\beta,R) \;, \tag{B11}$$

where f_o = the oscillator strength of the undisplaced component,

F_o = the "normal" field strength,

$= 1.1601\ (P_e \theta)^{2/3}$,

$f_{\pm}$ = the oscillator strength of the displaced components (red denoted by + and violet by −),

and $I(\beta,R)$ is expressed as a series expansion (see Evans 1966). The first term in equation (B11) is the broadening function for the central component and the second term is for the displaced components which is taken from the work of David (1961) for the Stark broadening. The detailed expression including an allowance for resonance broadening is obtained from Evans (1966). The arguments of the function I are the ratio R of the half-width for the mean ion field to that for electron and resonance broadening and the displacement β from the line center in units of the normal field displacement.

e) The Theoretical Curve of Growth and Computational Procedure

The theoretical curve of growth was explained in Section III. The quantity $\log L_\lambda(\chi)$ in equation (2) of that section is related to $\log L_\lambda^*$ used by Aller, Elste, and Jugaku (1957) by

$$\log L_\lambda(\chi) = \log L_\lambda^* + \Delta\chi\theta_a. \tag{B12}$$

where θ_a = an "excitation" temperature representative of the atmosphere of interest.

The saturated equivalent width is computed from the line depth equation (B2) by

$$\left[\frac{W}{\lambda}\right] = \frac{1}{\lambda}\int_0^{+\infty} R\, d\lambda\ . \tag{B13}$$

The actual integration is only carried out over a finite range in as much as the line depth becomes extremely small at large $\Delta\lambda$ for weak and medium strong lines.

A brief explanation of the procedure used in the computations of the theoretical curve of growth will now be given. All quantities that depend only on the atmospheric model are computed first. The quantities include factors that are used in the Boltzmann and Saha equations. Then the quantities that depend on the wavelength region are calculated. This involves a conversion of quantities obtained from the model atmosphere calculations into the proper form to be used later in the line calculations. Next an interpolation is performed on the partition functions that will be needed to calculate the line absorption coefficient. After the partition functions have been obtained the depth dependent integrand for the line optical depth equation (B9) is calculated. Then log C_λ equation (1) is calculated. Finally the saturated equivalent width equation (B13) is obtained by integrating the line depth equation (B2) over wavelength. The computer programs that were used to make these calculations were written by Evans (1970).

ACKNOWLEDGEMENT

The author would like to express his sincere thanks to Dr. John C. Evans for the suggestion of the problem, for his guidance and assistance in the work, and for the use of his computer programs. He would also like to thank the Computer Science Department at Kansas State University for making computer time available for this project. Support for this study was provided by a N.D.E.A. Traineeship and a part time teaching assistantship in the Physics Department.

REFERENCES

Aller, L. H. 1963, Astrophysics: The Atmospheres of the Sun and Stars (New York: Ronald Press Co.).

Aller, L. H., Elste, G., and Jugaku, J. 1957, Ap. J. Suppl., 3, 1.

Avrett, R. and Krook, M. 1963, Ap. J., 137, 874.

Babcock, H. 1949, Ap. J., 110, 126.

_______. 1958, Ap. J. Suppl., 3, 141.

_______. 1962, Astronomical Techniques, ed. W. A. Hiltner (Chicago: The University of Chicago Press), Chap. 5.

Baschek, B. and Oke, J. B. 1965, Ap. J., 141, 1404.

Beckers, J. M. 1969, Solar Phys., 9, 372.

Boyarchuk, A. A., Efimov, Yu. S., and Stepanov, V. E. 1961, Sov. Astr., 4, 766.

Bray, R. J. and Loughhead, R. E. 1964, Sunspots (Great Britain: Pitman Press).

David, K. 1961, Z. Astrophys., 53, 37.

Durrant, C. 1970, Mon. Not. R. Astr. Soc., 147, 59.

Elste, G. 1968, Solar Phys., 3, 106.

Evans, J. C. 1966, thesis (Ann Arbor: University of Michigan).

_______. 1969, Bull. Am. Astr. Soc., 1, 276.

_______. 1970, unpublished research.

Gingerich, O. 1964, Proceedings First Harvard - Smithsonian Conference on Stellar Atmospheres, p. 17.

_______. 1969, Theory and Observation of Normal Stellar Atmospheres (Cambridge: M. I. T. Press), p. 394.

Glagolevskii, Y. 1967, Soviet Astr., 10, 955.

Corliss, C. H., and Bozman, W. R. 1962, NBS Monograph No. 53 (Washington D. C.: Department of Commerce).

Corliss, C H., and Tech, J. L. 1968, NBS Monograph No. 108 (Washington, D. C.: Department of Commerce).

Griem, H. R. 1964, Plasma Spectroscopy (New York: McGraw-Hill Book Co.).

Gussman, E. A. 1967, Z. Astrophys., 65, 456.

Kourganoff, V. 1963, Basic Methods in Transfer Problems (New York: Dover).

Mihalas, D. 1965a, Ap. J. Suppl., 9, 321.

________. 1965 b, Ap. J., 141, 564.

________. 1966, Ap. J. Suppl., 13, 1.

________. 1967, Methods in Computational Physics (New York: Academic Press), Vol. 7, p. 1.

Moe, O. K. 1968, Solar Phys., 4, 267.

Moe, O. K. and Maltby, P. 1968, Astrophys. Lett., 1, 189.

Pecker, J. 1965, Annual Review of Astronomy and Astrophysics (Palo Alto: Annual Reviews, Inc.), Vol 3, p. 71.

Preston, G. W. 1967, Magnetic and Related Stars, ed. R. C. Cameron (Baltimore: Mono Book Corp.), p. 31.

Rachkovsky, D. N. 1961, Izv. Krym. Astrofiz. Obs., 25, 277.

Renson, P. 1967, Ann. Astrophys., 30, 697.

Sargent, W. L. 1966. Abundance Determinations in Stellar Spectra, ed. H. Hubnet (New York: Academic Press) p. 250.

Stepanov, V. 1958a, Izv. Krym. Astrofiz. Obs., 18, 136.

________. 1958b, Izv. Krym. Astrofiz. Obs., 19, 20.

________. 1960, Sov. Astr., 4, 603.

Underhill, A. and Waddell, J. 1959, NBS Circular 603 (Washington, D. C.: Department of Commerce).

Unno, W. 1956, Publ. Astr. Soc. Japan, 8, 108.

Unsold, A. 1955, Physik Der Sternatmospharen (Berlin: Springer-Verlag).

Warner, B. 1967, Mem. R. Astr. Soc., 70, 165.

Weidemann, V. 1955, Z. Astrophys., 36, 101.

Wolff, S. 1967, Ap. J. Suppl., 15, 21.

Wiese, W. L., Smith, M. W., and Miles, B. M. 1969 NSRDS-NBS 22 Vol. II (Washington, D. C.: Department of Commerce).

Wiese, W. L., Smith, M. W., and Glennon, B. M. 1966, NSRDS-NBS 4 Vol. I (Washington, D. C.: Department of Commerce).

THE EFFECTS OF A MAGNETIC FIELD ON ABUNDANCE DETERMINATIONS IN STELLAR ATMOSPHERES

by

CHARLES STEPHEN NICHOLS

B.S., University of Missouri at Rolla, 1968

AN ABSTRACT OF A MASTER'S THESIS

submitted in partial fulfillment of the

requirements for the degree

MASTER OF SCIENCE

Department of Physics

KANSAS STATE UNIVERSITY
Manhattan, Kansas

1970

In an effort to understand the apparent abundance anomalies found for the Ap stars, the intensification in equivalent width due to Zeeman broadening has been investigated for a grid of ten LTE model atmospheres covering the Ap star region of the HR diagram. The models were computed using a scheme due to Elste for a range in effective temperature from 10000° to $7200^{\circ}K$ with $\log g = 3.5$ and 4.0 and solar abundances. The model temperature distributions were taken from the grid of constant flux radiative models by Mihalas.

Theoretical curves of growth for the models were obtained by integrating detail line profiles computed for an LTE source function using a gradient method similar to that of Gussman. Zeeman broadening was treated with a modified version of the Stepanov theory with broadening of individual Zeeman components by thermal and pressure mechanisms. Curves of growth were calculated for selected lines of C I, Si I, Si II, Fe I, Fe II, and Eu II from which a maximum overabundance can be determined resulting from line intensification for the transverse Zeeman effect and various field strengths. The measured overabundances between the magnetic and non-magnetic curves of growth vary from factors of two to six depending upon the element and transition involved.